โครงการ

การเรียนการสอนเพื่อเสริมประสบการณ์

ชื่อโครงการ   ผลกระทบของอุณหภูมิร่างกายที่มีต่อคุณสมบัติของเสียงสะท้อนจากหูชั้นในแบบเกิดขึ้นเองจากตุ๊กแกบ้าน

The effects of body temperature on the characteristics of spontaneous otoacoustic emissions from tokay gecko

ชื่อนิสิต   นายธนวัฒน์ งามพัตราพันธุ์   **เลขประจำตัว** 5933425823

ภาควิชา   ฟิสิกส์
ปีการศึกษา   2562

คณะวิทยาศาสตร์ จุฬาลงกรณ์มหาวิทยาลัย

The effects of body temperature on the characteristics of spontaneous otoacoustic emissions from tokay gecko

Mr. Tanawat   Ngampattrapan

A report submitted to Department of Physics of Chulalongkorn University in partial fulfillment of the requirements for the degree of Bachelor of Science in Physics

Academic Year 2019

Project Title: The effects of body temperature on the characteristics of spontaneous

otoacoustic emissions from tokay gecko

Author: Tanawat Ngampattrapan

Supervisor: Dr. Yuttana Roongthumskul
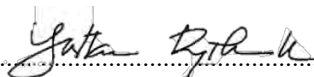
Field of Study: Physics

Academic year: 2019

This report is submitted to Department of Physics of Chulalongkorn University in partial fulfillment of the requirements for the degree of Bachelor of Science in Physics

This report has been approved by the committee:

……………………………………………………   Chairman

(Assistant Professor Dr. Panadda Dechadilok)

……………………………………………   Project Advisor

(Dr. Yuttana Roongthumskul.)

……………………………………………   Committee

(Dr. Thiparat Chotibut)

Project title:	The effects of body temperature on the characteristics of spontaneous otoacoustic emissions from tokay gecko
Author:	Tanawat Ngampattrapan
Field of Study:	Physics
Supervisor:	Dr. Yuttana Roongthumskul.
Academic year:	2019

Abstract

Spontaneous Otoacoustic emissions (SOAEs) are low-level sounds emitted from the ear in the absence of acoustic stimulations. The generation mechanisms of SOAEs are currently undetermined. However, several evidences indicate that SOAEs may be produced from hair cells, the acoustic receptors of the inner ear. Each hair cell has been mathematically described by a nonlinear oscillator that operates on a verge of an instability. We hypothesize that changing of the body temperature alters the level of random fluctuations in the inner ear, which in turn can strongly influence the dynamics of hair cells. This project aims to provide a further evidence that hair cells are responsible for the production of SOAEs by investigating the effects of changes in the body temperature on the spectrum of SOAE. We showed that the frequency of SOAEs increased with the body temperature at a rate of 30 to 130 Hz/$^\circ$C. The effect was stronger for emissions observed at higher frequencies. The amplitudes of SOAEs reached a maximum at the temperature levels between 28 and 30°C. Experimental results were compared with results from numerical simulations of a nonlinear oscillator near a supercritical Hopf bifurcation in the presence of noise. The oscillation frequency of a non-isochronous oscillator increased with the noise intensity. However, the model cannot capture the frequency-dependent temperature sensitivity, nor the alteration of SOAE amplitude observed in the experiment. Our results suggest that the generation of SOAEs is partly consistent with a non-isochronous nonlinear oscillator. A more complete development of the model is required to capture the experimental observations.

Acknowledgement

Contents

Chapter 1

Introduction

1.1 Background and motivations

Hearing disorders are one of the most common health problems in Thailand. In 2018, World Health Organization (WHO) has estimated that 6.1% of the world's population live with disabling hearing loss. This includes over 2 million people in Thailand [30]. The progressively increasing prevalence of hearing loss requires more effective assessment tools as well as treatments. To date, there are a limited number of diagnostic methods for hearing disorders, for example, the audiometry test, the otoacoustic emission (OAE) test, and the auditory brainstem response (ABR) test. Although these test results can indicate the presence of auditory impairments, further interpretations on the compromised mechanisms remain limited. This is mainly due to an insufficient knowledge on how the physical measurements arise from the inner ear.

Otoacoustic emissions (OAEs) refer to low-amplitude sounds emitted by the inner ear which can be measured by inserting a sensitive probe microphone into the ear canal. OAEs is a common noninvasive method used in the study of the inner ear's mechanisms. In a quiet environment, the inner ear produces an acoustic energy detectable in the outer ear, termed spontaneous otoacoustic emissions (SOAEs). The amplitude spectrum of an SOAE signal displays several peaks whose frequencies and amplitudes varies from species to species and animals to animals (**Figure 1.1**). SOAEs have been detected in all classes of vertebrates e.g. human, guinea pig, most reptiles, barn owl, and frogs [1-7]. Through an unknown mechanism, the spontaneous emissions originate from the interplay between the nonlinear properties and the amplification processes of hair cells, the acoustic sensors of the auditory system. Therefore, investigations of SOAEs under different types of manipulations should help elucidate the activities of hair cells in the absence of stimulus.
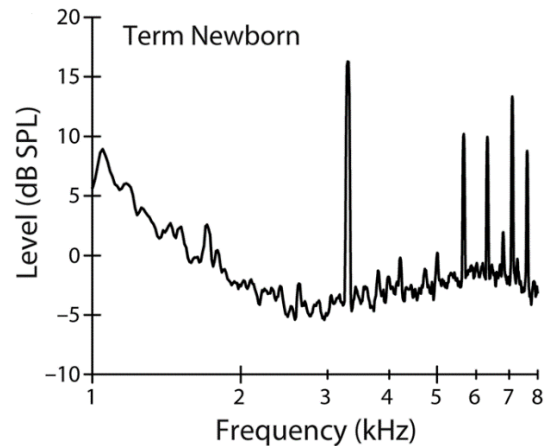
Figure 1.1 An example of SOAEs from newborn human. The number and amplitude of SOAEs decrease with age [1].

Signal transduction of the auditory system is performed by hair cells, each comprises of two parts: the cell body and the hair bundle. Upon an impact of an acoustic wave, hair bundles are deflected resulting in the opening of mechanically gated ion channels. The influx of anions depolarizes the membrane potential and consequently triggers the release of neurotransmitters at the synapses located at the base of the cell. Under *in vitro* condition, hair bundles can oscillate spontaneously under an appropriate range of calcium concentrations (**Figure 1.2**). The bundle displacement has been mathematically described by nonlinear systems poised near a bifurcation between a quiescent behavior and a limit-cycle oscillation [9].

Figure 1.2 The displacement of a hair bundle from the bullfrog sacculus transitions from a quiescent to an oscillatory behavior upon an increase in the concentration of calcium [9].

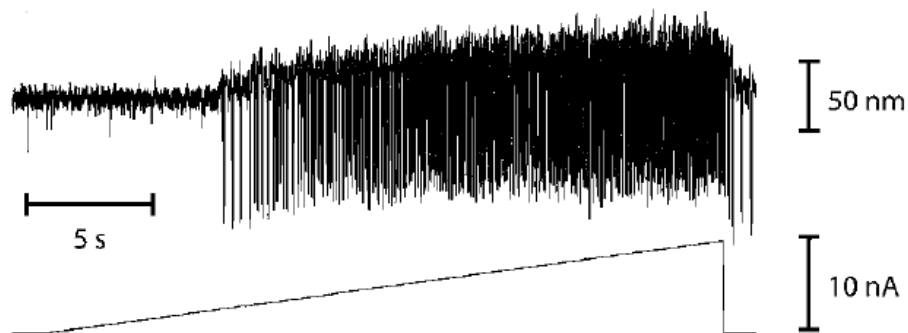One of the accepted theories for SOAE generation hypothesizes that the spontaneous oscillations of hair bundles create sufficiently high acoustic energy that can be measured as SOAE signals. In the view of this theory, manipulations of hair bundles should directly alter the characteristics of SOAEs. For example, changing calcium concentration inside the inner ear evokes a shift in the emission frequencies [18].

There are reports on the effects of body temperature on SOAEs in several ectotherms, e.g. frogs and lizards [4,12-14]. SOAE frequency tend to increase with body temperature, and the emissions with higher frequencies have larger shifts. On the other hand, the amplitude of SOAE does not show a clear relationship with temperature [13]. We hypothesize that changing of the body temperature alters the level of random fluctuations in the inner ear. As the motions of hair bundles are subject to noises from various sources [19], their dynamics could be greatly influenced upon changing of the noise level.

When a nonlinear oscillator is poised on the stable regime near a bifurcation point, external noise can induce an oscillation at a certain frequency [11, 17]. In some cases, the width of a peak in the spectrum can be minimized at a suitable noise amplitude, a phenomenon termed coherence resonance. Studying the effects of noise intensity on the spectral peak of a nonlinear oscillator may help us understand the relationship between SOAEs and temperature level and give us a better picture of the production mechanism of SOAEs.

This project will investigate the characteristics of SOAE spectra at different temperature levels and develop a mathematic model to describe the experimental results. The animals used in this project are tokay geckos (*Gekko gecko*), an ectotherm species that produces strong SOAEs. The model is a nonlinear oscillator that shows supercritical Hopf bifurcation with a noise term. Comparison of the experimental and theoretical results will provide further evidence for the consistency between the generation of SOAEs and nonlinear oscillators.

1.2 Objective

1. To study the effects of body temperature on the characteristic of spontaneous otoacoustic emissions from tokay gecko (*Gekko gecko*).

2. To study the effect of noise on a nonlinear oscillator near a supercritical Hopf bifurcation to describe the effects of body temperature on SOAEs

Chapter 2

Background Theory

2.1 Structure and properties of hair cell
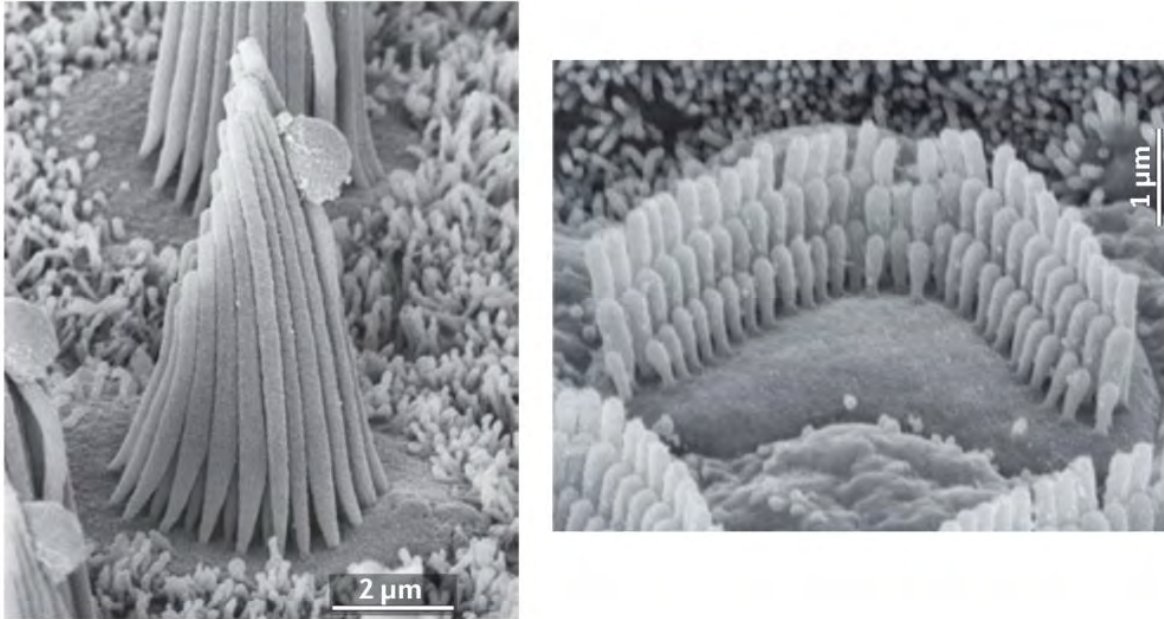
Figure 2.1 Images of hair bundles from a bullfrog sacculus (left) and a rat cochlea (right) from scanning electron microscope [21].

Hair cells in the inner ear detect sound stimuli and send electrical responses to the brain. A hair cell consists of a cell body and a bundle. The cell body is embedded in the epithelium and is innervated by an afferent nerve; therefore, its function is to send the response to the brain. The hair bundle is a pack of cilia arranged in rows graded by their height. The tip of a shorter cilium is connected to the side of the taller cilium by a filament called tip link. The hair bundle is deflected in response to an acoustic stimulus. This leads to a change in the tension of the tip link which subsequently alters the opening probability of the mechanically gated ion channel on the cilia. The membrane potential is then modified, and the action potential is generated and sent to the brain.

When a constant force is applied to a hair bundle, the magnitude of the bundle displacement displays a nonlinear relationship with the force. By taking the derivative of the displacement with respect to the force, the bundle stiffness appears to possess a minimum at zero displacement. In addition, within a suitable range of calcium concentrations, the stiffness can be decreased and become negative. The system thus becomes unstable and displays a self-sustained oscillation [15,21]. This spontaneous oscillation may underly the generation of SOAEs.

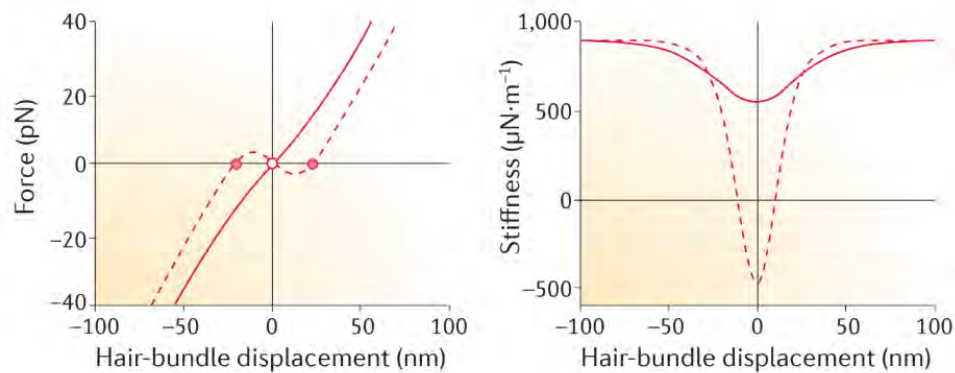**Figure 2.2** The relationship between (Left) the magnitude of a constant force applied on the hair bundle and (Right) the bundle's stiffness as a function of bundle's displacement. The thick line depicts the stiffness at low calcium concentration and the dashed line is obtained from high calcium level [21].
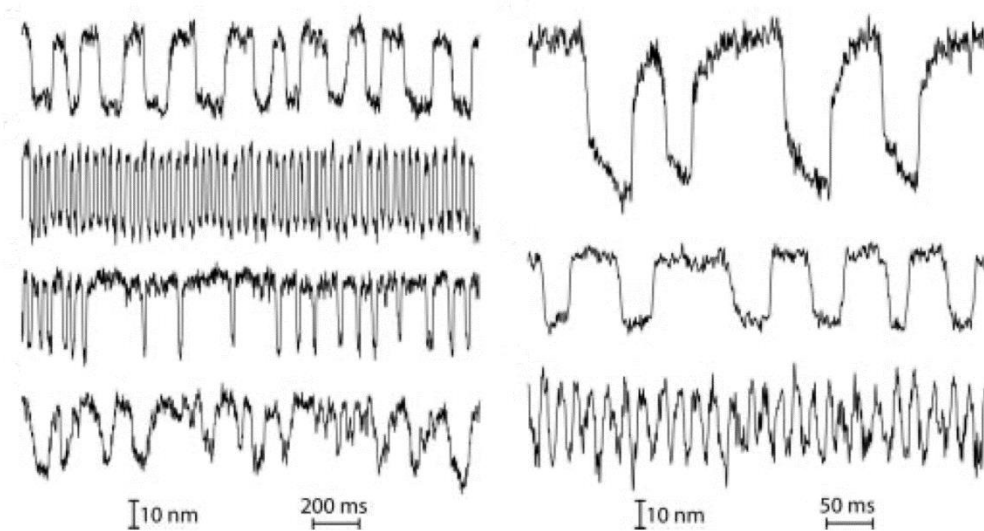

Figure 2.3 Examples of spontaneous oscillations of hair bundles from the Bullfrog sacculus [15]

2.2 Anatomy of inner ear of Tokay gecko

The ears of tokay gecko are located behind the eyes and appear as a shallow ear canal terminated by the eardrums. The hearing organ in the inner ear is the basilar papilla. (**Figure 2.4**). Hair cells are arranged on the papilla in rows of approximately 2000 μm in length and 120 μm in width. The papilla is situated on top of the basilar membrane which is connected to the Limbic cartilage. The nerve fibers enter the papilla from one side called the neural edge and innervate hair cells on the opposite side called the abneural edge.

Hair cells within the one-third length from the entrance to the basilar papilla are responding to the sound frequency below 1000 Hz. The rest of the papilla is sensitive to sounds of frequencies from 1000 to 5000 Hz. In this region, hair cells are aligned in order of their characteristic frequencies. Hair cells are divided into 2 strips. Those on the neural edge are covered by a single band of extracellular tissue called the tectorial membrane. The tectorial membrane is connected to a cartilage, Limbic tip, via a tectorial curtain. On the abneural edge, each transverse row of hair cells is covered by a single tissue called sallet, each connected to the two adjacent neighbors by a thin filament.
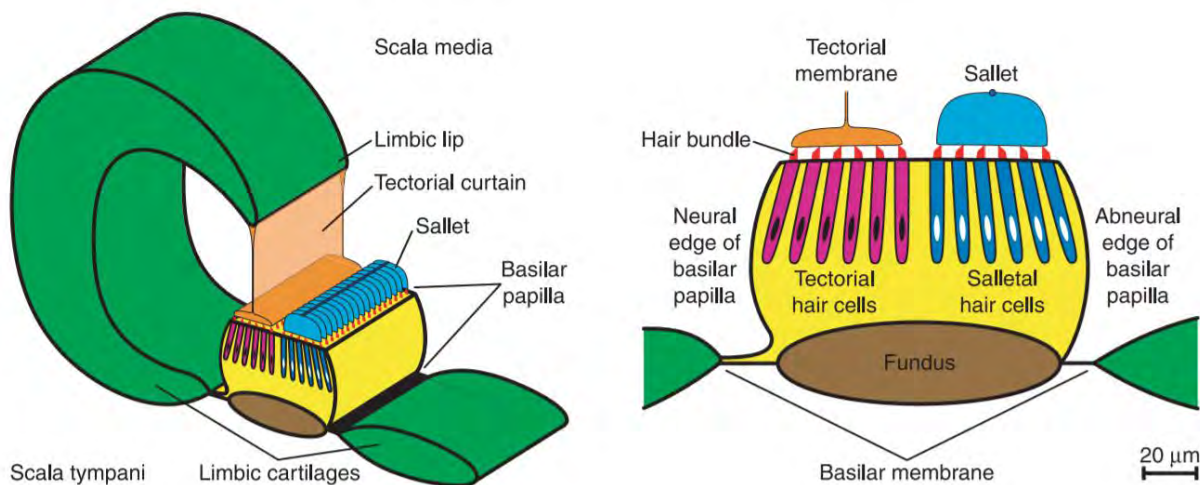

Figure 2.4 The anatomy of basilar papilla in the inner ear of tokay gecko [22].

Hair cells from each strip are suggested to perform different functions. In the abneural edge side, the nerve fibers are connected to the hair cells. So, their function is likely to transduce the mechanical signal into electrical signal. On the other hand, hair cells from neural side may act as an amplifier.

2.3 Spontaneous otoacoustic emissions in Tokay gecko

The auditory organs of many vertebrates are not only receiving sounds but also creating ones. These sounds can be detected by placing a sensitive microphone near the eardrum in a quiescent environment. Typically, the emitted sounds are within the same frequency range as the hearing sensitivity of the animal. These sounds, called spontaneous otoacoustic emissions or SOAEs, have been detected in all classes of vertebrates including lizards such as tokay gecko. The amplitude spectrum of SOAEs typically displays ~10 peaks from 1,000 Hz to 5,000 Hz with the amplitude from -6 dB to 10 dB (**Figure 2.5**).
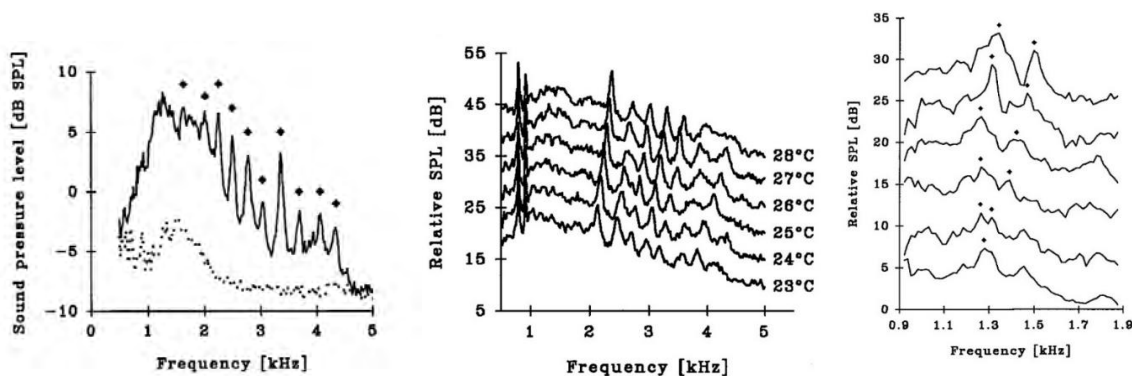
Figure 2.5 (Left) The spectrum of SOAEs from tokay gecko compare to noise level (dotted line). The dots indicate the center frequency of a peak. (Middle) SOAE amplitude spectra show a positive frequency shift when raising body temperature. (Right) Some SOAE peaks split into 2 peaks. The dots indicate the center frequency of the peaks [14].

SOAEs are sensitive to temperature. When the body temperature of a gecko was raised, SOAE peaks in the amplitude spectrum shift towards higher frequency. The magnitude of the shift depends on the body temperature as well as the center frequency of the peak. The largest frequency shifts have been observed over the range of body temperature between 25 and 28 °C.

In addition, SOAEs with higher frequencies display larger shifts. Occasionally, an SOAE peak may split into 2 peaks upon an increase in the temperature.

Figure 2.6 The frequency shifts of SOAEs measured at different body temperature intervals from *G. gecko* (filled circle) and *E. macularius* (opened circle) [14].

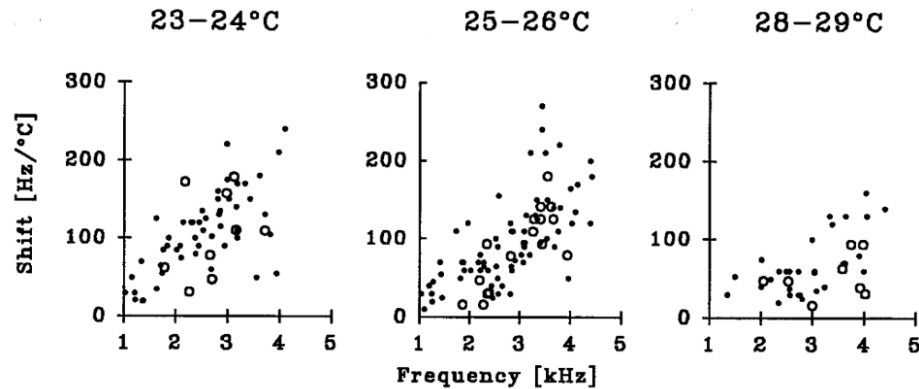## 2.4 Supercritical Hopf bifurcation

Supercritical Hopf bifurcation have been employed in describing the dynamics of the inner ear [25] and single hair bundles [26]. Spontaneous oscillations exhibited by a hair bundle can be brought to a suppression upon several types of perturbations such as changing of calcium concentration [9], or an attachment of an external loading that alters the mass or stiffness of the bundle [15].

The behaviors of spontaneous oscillations in the transition regime under different manipulations have been demonstrated to match a nonlinear system crossing distinct types of bifurcation such as a Hopf, or a saddle node on an invariant circle (SNIC) bifurcation [27, 28]. When loaded by an elastic element or a mass, the bundle's displacement displays a supercritical Hopf bifurcation [29]. These manipulations most likely resemble the physiological conditions experienced by hair cells within the inner ear, rendering a supercritical Hopf bifurcation an appropriate mathematical description.

Supercritical Hopf bifurcation occurs when a system transitions from a quiescent to an oscillatory behavior. The dynamic of the oscillator is governed by a control parameter. The general equation of a nonlinear oscillator near a supercritical Hopf bifurcation is

$$\dot{z} = (\mu + i\omega_0)z - (\alpha + i\beta)|z|^2 z \tag{2.1}$$

z is a complex number. μ is the control parameter. ω_0 is the characteristic frequency, $\alpha + i\beta$ is the complex coefficient that governs the degree of nonlinearity of the system. This system displays a supercritical Hopf bifurcation when $\alpha > 0$.

From the equation (2.1), the fixed point of the system is at $z = 0$. If we let $z = x + iy$, the equation (2.1) can be written as.

$$\dot{x} = \mu x - \omega_0 y - [(\alpha x - \beta y)(x^2 + y^2)]$$
$$\dot{y} = \omega_0 x + \mu y - [(\beta x + \alpha y)(x^2 + y^2)] \tag{2.2}$$

A linearization at the fixed point $z = 0$ yields the Jacobian of equation (2.2) as follows

$$A = \begin{pmatrix} \mu & -\omega_0 \\ \omega & \mu \end{pmatrix}$$

Which has eigenvalues of $\lambda = \mu \pm i\omega_0$. When the real part of the eigenvalue is negative, or when $\mu < 0$, the fixed point is a stable spiral fixed point. A trajectory initially placed at an arbitrary point in the phase scape will spiral towards the fixed point. For $\mu > 0$, the fixed point becomes an unstable spiral fixed point. The system will spiral outward to a limit cycle (**Figure 2.7**). A supercritical Hopf bifurcation is defined when a stable fixed point becomes unstable with an emergence of a stable limit cycle in the phase space, which in this case occurs at mu = 0.
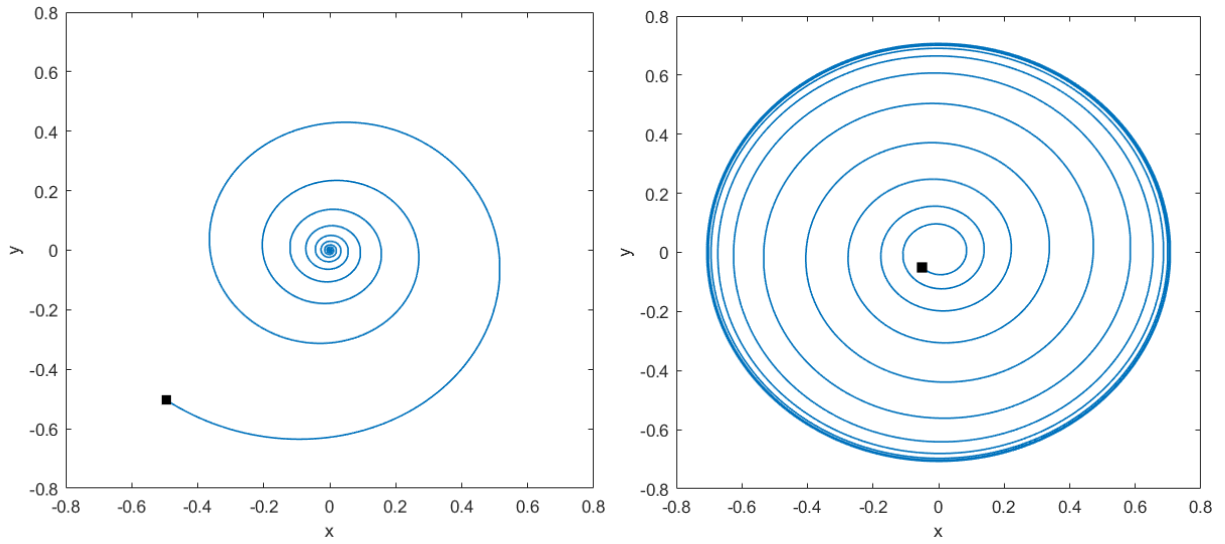
Figure 2.7 The phase space of supercritical Hopf bifurcation for (left) $\mu < 0$ and (right) $\mu > 0$. Filled squares indicate the initial positions.

Chapter 3

Methodology

This project was divided into 2 parts. First, we measured SOAEs from tokay gecko and studied the effects of alterations in the body temperature on their characteristics. In the second part, we developed a mathematical model to describe the experimental observations.

3.1 Experimental setup

Experiments were performed in an anechoic chamber. The setup was inside an acrylic box whose walls lined with acoustic foam sheets. The schematic diagram of apparatus shows in **Figure 3.1**.
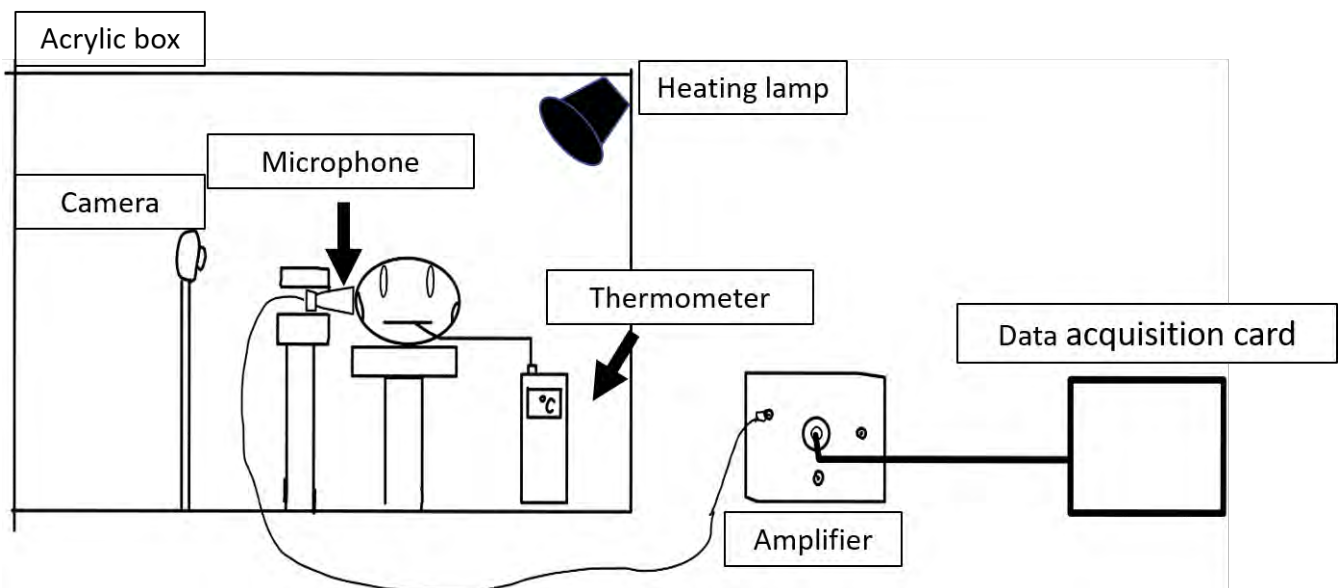

Figure 3.1 shows the schematic diagram of recording apparatus.

Tokay geckos (*Gekko gecko*) of both sexes were obtained from Department of Biology, Chulalongkorn university. The body weight ranged from 60 to 120 g. The animals were anesthetized with Sodium-Pentobarbital (Nembutal) at 20-25 mg/kg body weight via an

intraperitoneal injection. After the loss of righting reflex, typically ~20 minutes after the drug administration, the animal was transferred into the setup where SOAEs from the right ear was recorded. A hollow plastic cylinder was used as an artificial ear canal, whose one end connected to the sensitive microphone (ER10), and the other covered the tympanum. The gap between the cylinder and the animal's skin surrounding the eardrum was filled with petroleum jelly (Vaseline^{TM}). The body temperature was measured by inserting a thermocouple inside the mouth.

Starting from ~25 $^{\circ}$C, the temperature inside the acrylic box was continuously increased by a heating lamp. The maximal ambient temperature achieved by our setup was ~33 $^{\circ}$C. After the animal's temperature reached 31 $^{\circ}$C, the heating lamp was turned off, and the setup was then cooled down passively by opening the acoustic foam covers to increase the ventilation. The experiment was repeated until the animal recovered from anesthesia. SOAEs were recorded whenever the body temperature changed by 0.5 C. Signals from the microphone were collected by a data acquisition card and converted into digital signals by an A/D converter at 50 kHz sampling rate.

3.2 Signal analysis

All analyses were performed in MATLAB. The recorded signals were strongly influenced by noises from the animal's breathing, each typically lasted 10 ms. In order to exclude these intermittent perturbations, an artifact rejection algorithm was applied to the signal before further analyses. First, the signal was divided into non-overlapping segments, each was 0.1 second long. Then, we identified the maximum sound pressure from each segment and calculated the average and standard deviation of these maximal values. Any segments whose maxima exceeded the average by at least twice the standard deviation were rejected from the analysis. The algorithm was then repeated twice to ensure that all artificial peaks in the pressure were eliminated.

We then calculated the amplitude spectrum of the signal. We multiplied each remaining segment by a Hanning window in equation (3.1), and calculated the complex spectrum using Fast

Fourier Transform (FFT) technique. The amplitude spectrum of the signal was obtained from the average magnitude of the spectra.

$$w(n) = 0.5(1 - \cos(\frac{2\pi n}{N})) , 0 \leq n \leq N \tag{3.1}$$

where N is the number of data point in each segment.

The spectrum of SOAEs consisted of several broad-band peaks. To detect the spectral peaks, we identified all the local maxima and minima. A local maximum whose pressure level was higher than the two neighboring local minima by 1.0 dB was identified as an SOAE peak.

We extracted three characteristics of an SOAE peak: the center frequency, the width, and the height. First, all data points between the two adjacent local minima surrounding a peak was fitted with a Lorentzian function in equation (3.2).

$$y(x) = \frac{a}{(x - x_0)^2 + \sigma^2} + c \tag{3.2}$$

Where a, x_0, σ, and c are fitting parameters. The center frequency was x_0. The width was measured at 0.5 dB below the peak, and is given by $2\sqrt{\frac{a\sigma^2}{a - \sigma^2 d} - \sigma^2}$ where d is y at 0.5dB below the peak. To identify the peak height, an SOAE spectrum was compared to that of a signal recorded from the animal's skin next to the ear. This provided an estimate of the noise floor of the recordings. The peak height was calculated from the difference between the peak pressure and the noise floor at the same frequency.
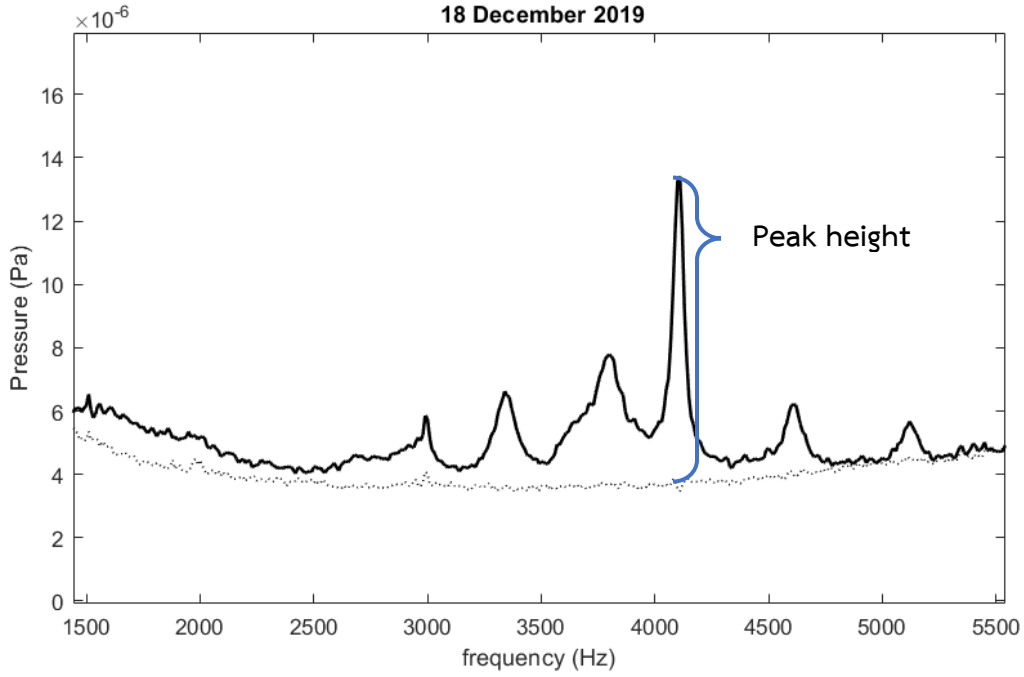
Figure 3.2 shows the spectrum of SOAEs and the noise floor. The peak height was calculated from the difference between the peak pressure and the noise floor.

3.3 Developing mathematical model

A mathematical model used to describe the effects of temperature on SOAE characteristics was a nonlinear oscillator that displayed a supercritical Hopf bifurcation as follows,

$$\dot{z} = (\mu + i\omega_0)z - (\alpha + i\beta)|z|^2 z + D\xi(t) \tag{3.3}$$

Where $z = x + iy$ is complex number. x denotes the acoustic pressure measured from the eardrum. μ is the control parameter. ω_0 is the characteristic frequency. α, β are the coefficients that govern the degree of nonlinearity of the system. The noise amplitude is denoted by D and is proportional to a square root of temperature according to Stoke-Einstein relation. $\xi(t)$ represents a gaussian white noise term consisting of both real and imaginary part, $\xi(t) = \eta_r + i\eta_i$ which satisfies $\langle \eta_\alpha(t)\eta_\beta(0) \rangle = \delta(t)\delta_{\alpha\beta}$ where $\alpha, \beta = r, i$.

We performed the numerical simulations on MATLAB[TM] using a 4th order Runge-Kutta algorithm with a time step of 0.001 for 200 seconds. The solution $x(t)$ was divided into 10 segments, and the amplitude spectrum was obtained in a similar fashion as the experimental data. The peak in the spectrum of $x(t)$ was fitted by a Lorentzian function in equation (3.2) and extracted the center frequency, peak height, and width at half maximum.

To explore the possibility that stable hair cells may be responsible for the generation of SOAEs, we investigated whether noise-induced oscillations in a quiescent system can capture the experimental results, we chose the control parameter $\mu = -0.1$. In addition, at the end of our study, we also presented the preliminary results from a system in the oscillatory regime with $\mu = 0.1$. The parameters that controlled the degree of nonlinearity were fixed at $\beta = -10, \alpha = 1$. We varied D from 0.01 to 10, and ω_0 from 2π to 10π. The characteristic frequency was rescaled such that the lowest oscillation frequency in the model was 1 Hz. To match the experimental results, the oscillation frequencies may be multiplied by 2000.

Chapter 4

Results

4.1 Spontaneous otoacoustic emissions from tokay geckos

SOAEs were recorded from 6 tokay geckos. The dates of experiments and the geckos' body weights are shown in **table A1**. Examples of SOAE amplitude spectra, all recorded at 28 ˚C, are illustrated in **Figure 4.1**. The amplitude spectra varied in their number of peaks and loudness. SOAE peaks were observed in the frequency range from 2,000 Hz to 6,000 Hz, with their amplitude ranging between -10 dB and 5 dB.
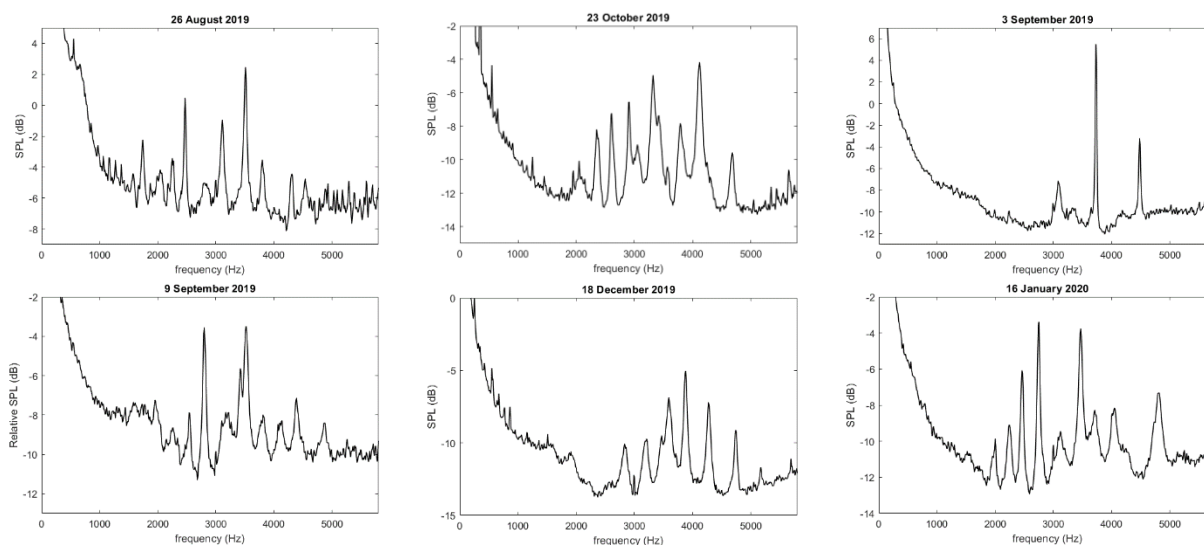

Figure 4.1 The spectrums of SOAEs from six geckos at 28 ˚C body temperature. Each title shows the date of recording.

SOAE spectra were sensitive to changes in the body temperature as shown in **Figure 4.2.** As the body temperature was increased, all peaks in the spectrum shifted towards higher frequency. The magnitude of the shift was frequency dependent: a peak with higher frequency displaced more than the lower one. The peak amplitude, on the other hand, displayed a more complex dependence on the body temperature. We found that some SOAE peaks emerged in the spectra as the body temperature increased, whereas some peaks were attenuated and

became indistinguishable from the noise floor. These effects were reversible upon decreasing the temperature.

To quantify the alterations of SOAE spectra, we extracted the characteristics of each SOAE peak in the amplitude spectrum by fitting a Lorentzian function. An example of the fit is shown in **Figure 4.3**. The center frequency and the peak width were determined from the fit, whereas the peak height was achieved by subtracting the noise floor recorded from the skin from the SOAE spectrum. We note that some SOAE peaks partially overlapped with a neighboring peak, and a single Lorentzian function could not capture the characteristic of the peak as illustrated in **Figure 4.3**. We excluded these peaks from the analysis.

4.2 Effects of body temperature on center frequency

Figure 4.4 shows a plot of the center frequency of one SOAE peak as a function of body temperature. In the low temperature range between 25 °C and 28 °C, the frequencies were identical during the heating and cooling process. However, a hysteresis was observed above 28 °C, in which SOAE frequency during the cooling was lower than the heating process. This feature could originate from the difference in the actual temperature of the inner ear and that monitored from the mouth cavity due to the heat capacity of the inner ear and the head. To minimize these effects, one would ideally maintain the temperature level until a thermal equilibrium was achieved before performing a measurement. However, as our experiments involved a continuous change in the temperature level, we focused on the data obtained from the heating process due to the lower rate of temperature change.
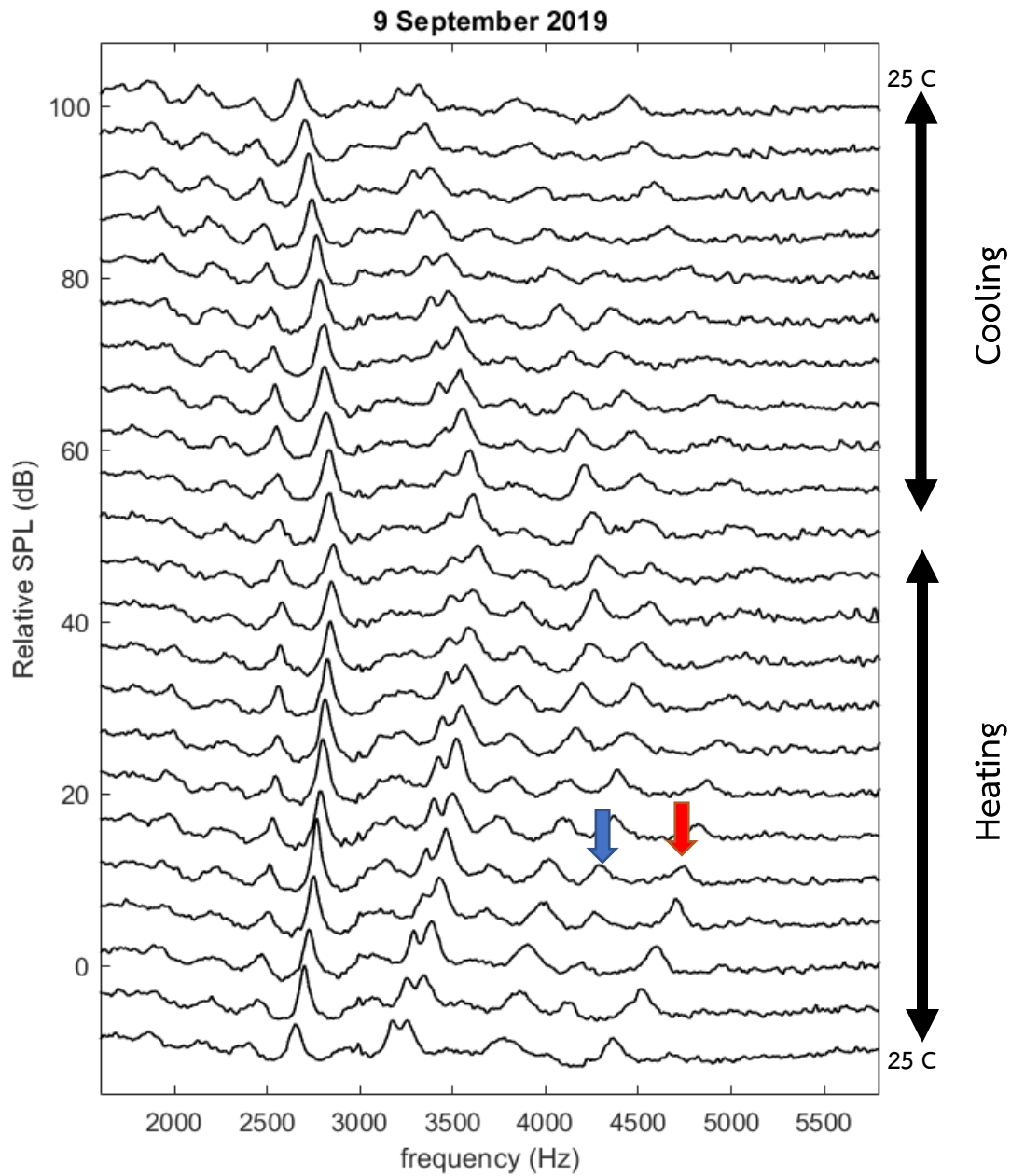
Figure 4.2 The waterfall plot of SOAE spectra at various levels of temperature during the heating and cooling processes. The blue arrow indicates an emerging peak, the red arrow indicates a peak diminished from the spectrum as the temperature increased.
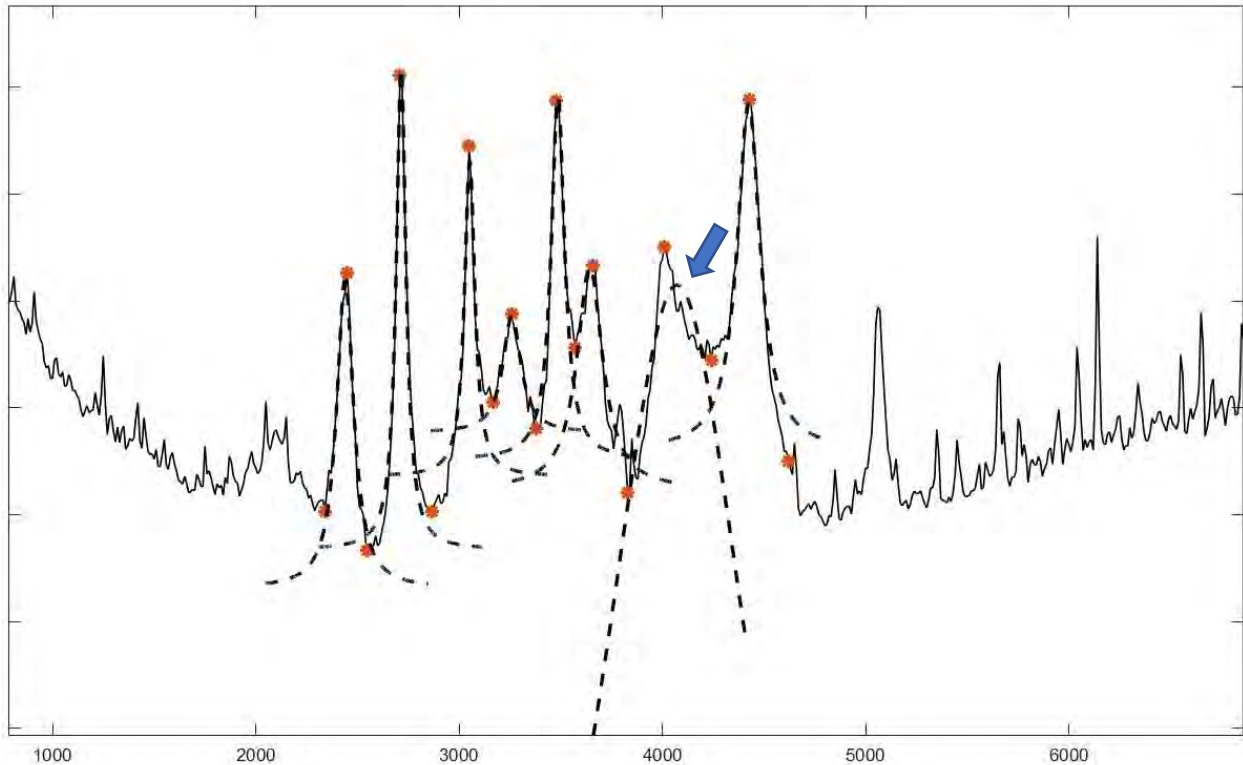
Figure 4.3 The fitted SOAE peaks by a Lorentzian function (dash lines). Orange dots indicate local extrema of the spectrum. The arrow indicates the peak that cannot be captured by the Lorentzian function. Note that in this case, a peak detection algorithm was implemented to the amplitude spectrum between 2,000 Hz and 5,000 Hz.

The center frequencies of all SOAE peaks displayed a monotonic increase with body temperature. The frequency was typically linear over a broad range of temperature between 26 and 30 °C (**Figure 4.5**). Outside of this range, the dependence became weakly nonlinear. To determine the temperature sensitivity (df/dT), we extracted the slope of a linear fit to the center frequencies between 26°C and 30°C. The temperature sensitivity was defined as the slope of the linear function. When plotted against the emission frequency measured at room temperature, we found that the temperature sensitivity increased from 30 Hz/°C for SOAE at 2,300 Hz to 130 Hz/°C for SOAE at 4,500 Hz (**Figure 4.6**).
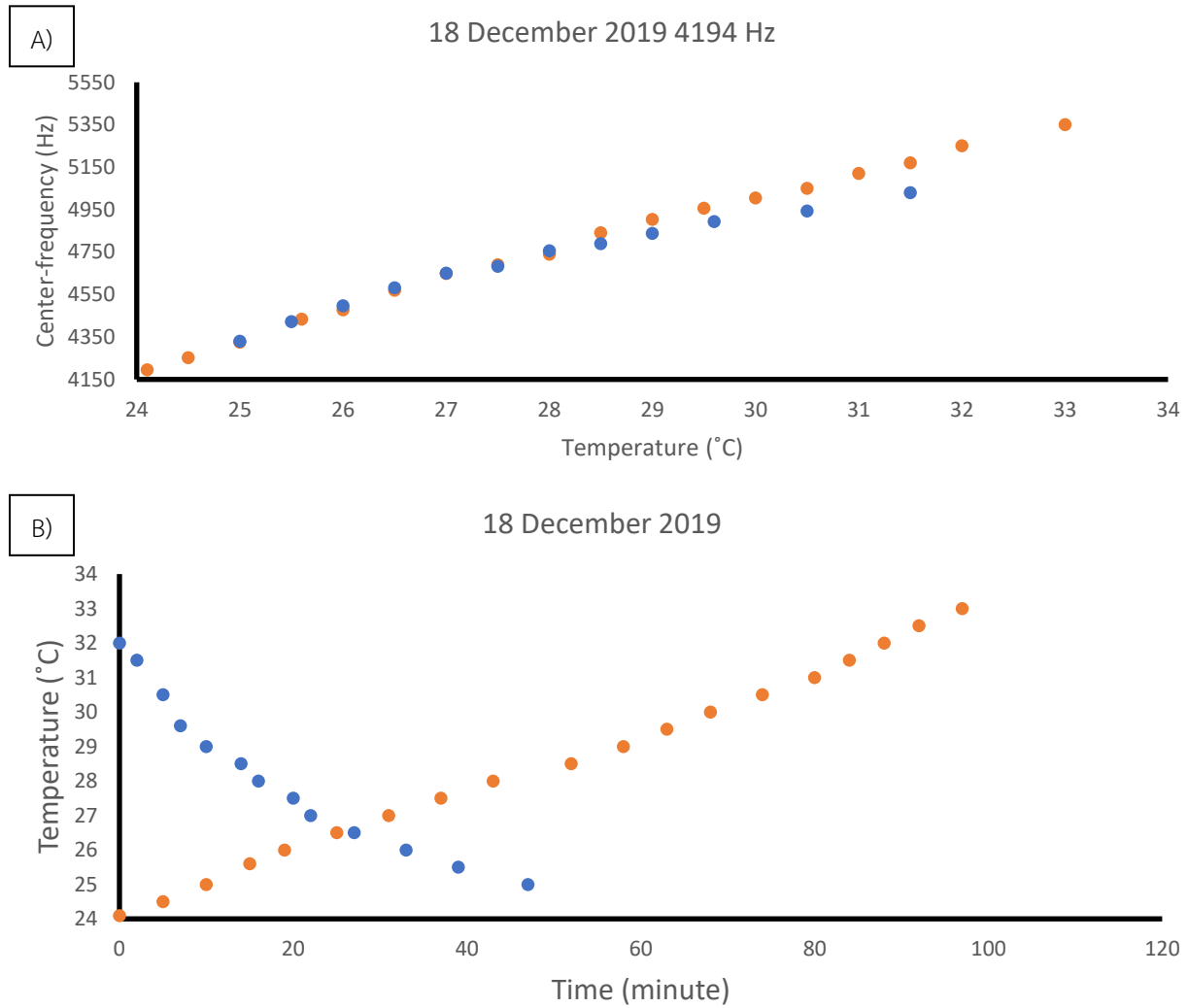
Figure 4.4 A) The center frequency during the heating (orange dots) and cooling process (blue dots). Above 28C, SOAE frequency during the cooling was less than the heating. B) The body temperature as a function of time after the beginning of each process. The change in body temperature in the heating process was slower than cooling.
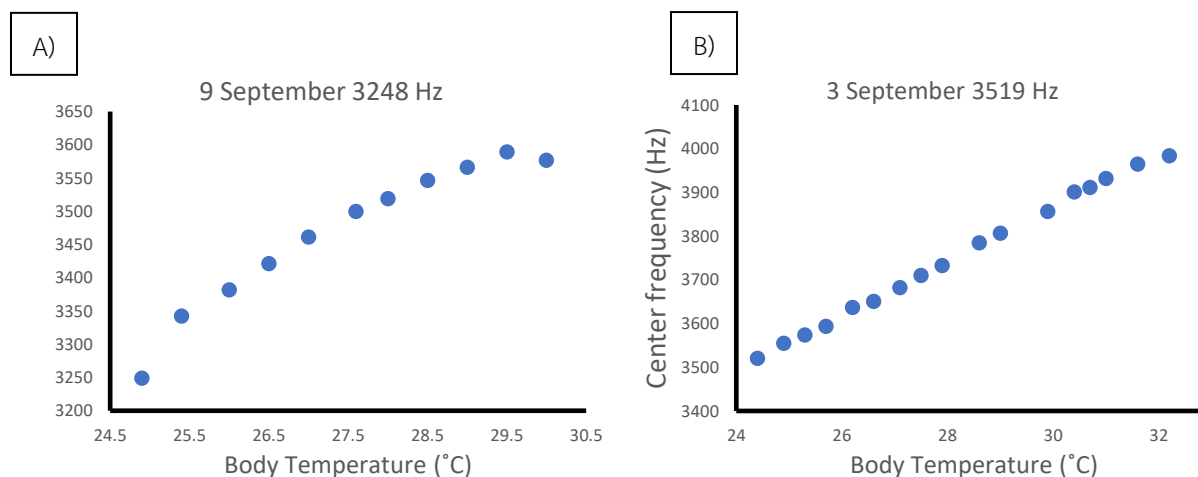
Figure 4.5 Relationships between center frequency and body temperature. A) The changes in the center frequency slightly decreased at higher body temperature. B) The relationship was relatively linear across the body temperature range.
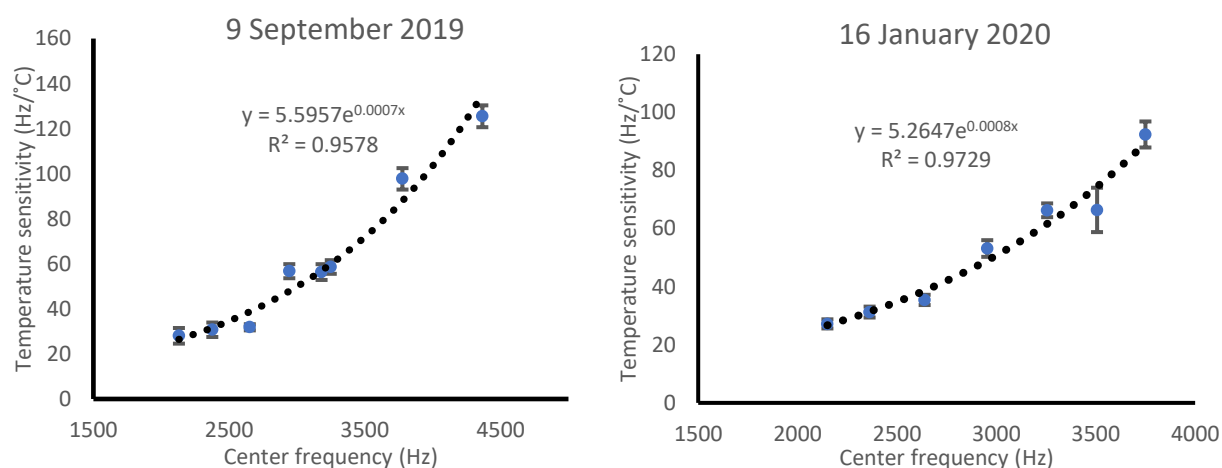
Figure 4.6 Temperature sensitivities versus the center frequency of the peak at 25 °C from two geckos show an exponential dependence. Black dotted lines indicate an exponential fit to the temperature sensitivity. Error bars are confidence intervals obtained from the linear fit.

4.3 Effects of body temperature on SOAE peak width and height

Unlike the center frequency, the temperature dependence of the peak width or height did not display a consistent trend. Three types of dependence are shown in **Figure 4.7**, with no obvious correlation with the emission level nor frequency.
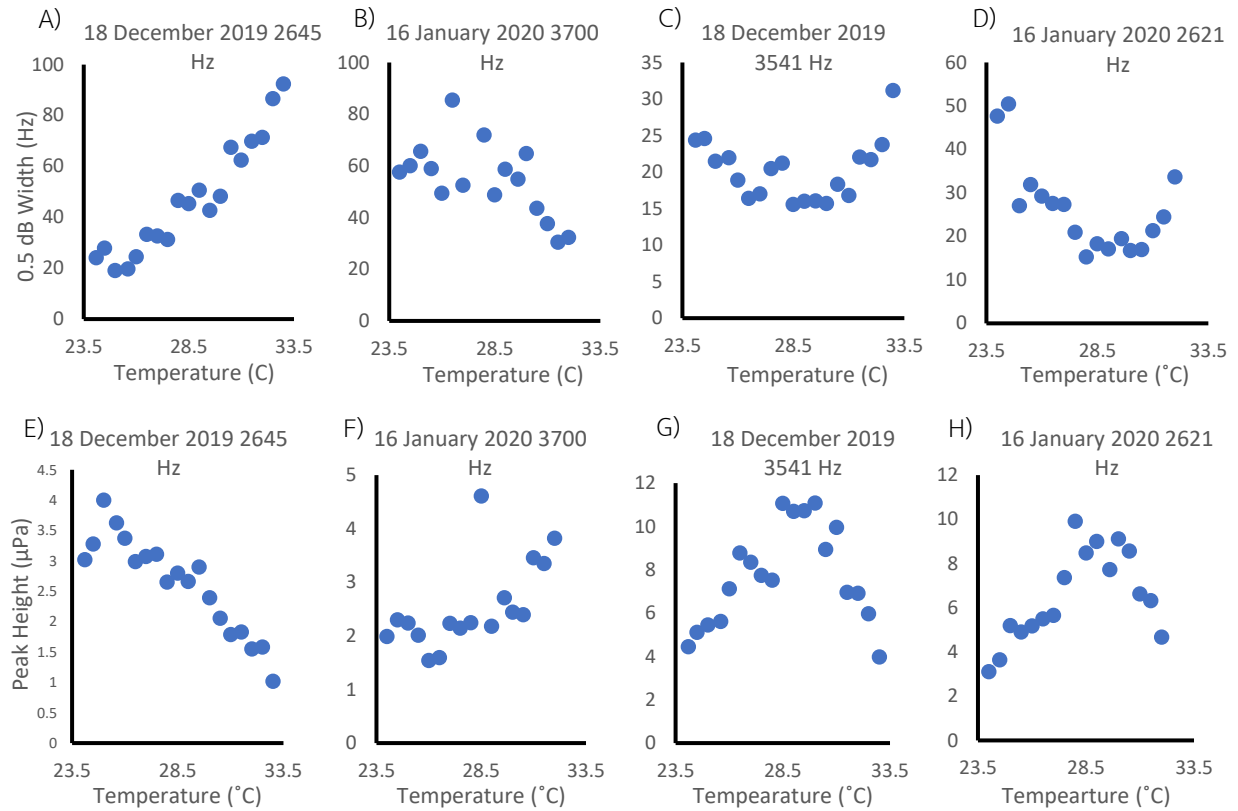
Figure 4.7 The relationship between SOAE width, peak height, and body temperature. A) The width increased with body temperature. B) The width decreased with body temperature. C) and D) The width displayed a minimum over a certain range of body temperature. E)-H) the peak height of peaks above shown the opposite relationship to the width.

We then investigated the relationship between the emission level and SOAE bandwidth. In **Figure 4.8**, we found that as the level increased, SOAE peak became sharper as indicated by the decline in the 0.5-dB bandwidth. This relationship was consistent in all peaks.

18 December 2019 2645 hz

Figure 4.8 SOAE peak width displayed a negative correlation with the peak height.

Numerical results

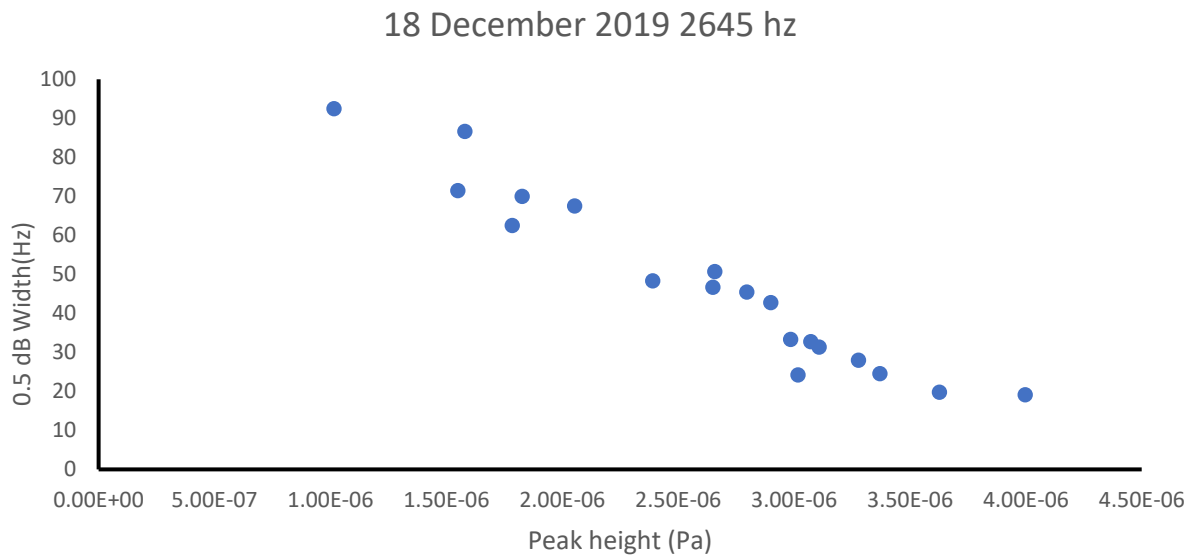Our mathematical model was based on a hypothesis that SOAEs were generated by the self-sustained vibrations of hair-cell bundles whose dynamics were subject to noises from various sources. An increase in the temperature might enhance the level of random fluctuations. Note that higher temperature also increased the rates of chemical reactions necessary for the active movement of hair bundles; however, we only focused on the effects of noise level in this work. We performed numerical simulations of a nonlinear oscillator near a supercritical Hopf bifurcation in the presence of noise. This oscillator was assumed to be non-isochronous, i.e., the oscillation frequency depended on the limit-cycle amplitude.

4.4 Nonisochronicity of supercritical Hopf bifurcation

From equation (2.1), by substituting $z = Re^{-i\varphi}$ into equation (2.1). the equation becomes

$$\frac{d}{dt}\left(Re^{i\varphi}\right) = (\mu + i\omega_0)Re^{i\varphi} - (\alpha + i\beta)R^3 e^{i\varphi}$$

$$e^{i\varphi}\frac{dR}{dt} + iRe^{i\varphi}\frac{d\varphi}{dt} = (\mu + i\omega_0)Re^{i\varphi} - (\alpha + i\beta)R^3 e^{i\varphi}$$

Matching real part and imaginary part we will have 2 equations

$$\frac{dR}{dt} = \mu R - \alpha R^3$$

$$\frac{d\varphi}{dt} = \omega_0 - \beta R^2$$

(4.1)

From these 2 equations, we can determine the oscillation amplitude and frequency. As mentioned above, there is a stable limit cycle when $\frac{dR}{dt} = 0$, then the amplitude is given by $R = \sqrt{\frac{\mu}{\alpha}}$ and the angular frequency follows $\omega = \omega_0 - \beta R^2$. We can see that the frequency depends on its amplitude when beta is not zero, a property of a non-isochronous system.

To investigate how random fluctuations may give rise to an oscillation, first we applied a transient force of 0.001 seconds to perturb the system in both quiescent and oscillation regime. The simulations were perform using $\mu = 0.01$, $\alpha = 1$, $\beta = -10$, and $\omega_0 = 2\pi$. In the quiescent regime ($\mu < 0$), the perturbation caused the system to displace from its stable fixed point and exhibited a prolonged damped oscillation. We performed Hilbert transform to extract instantaneous amplitude and instantaneous frequency. We found that the instantaneous frequency depends on the amplitude following the equation (4.1). When the oscillator was originally poised in the unstable regime, similar results were observed with the oscillation decayed towards a limit cycle (**Figure 4.9**).
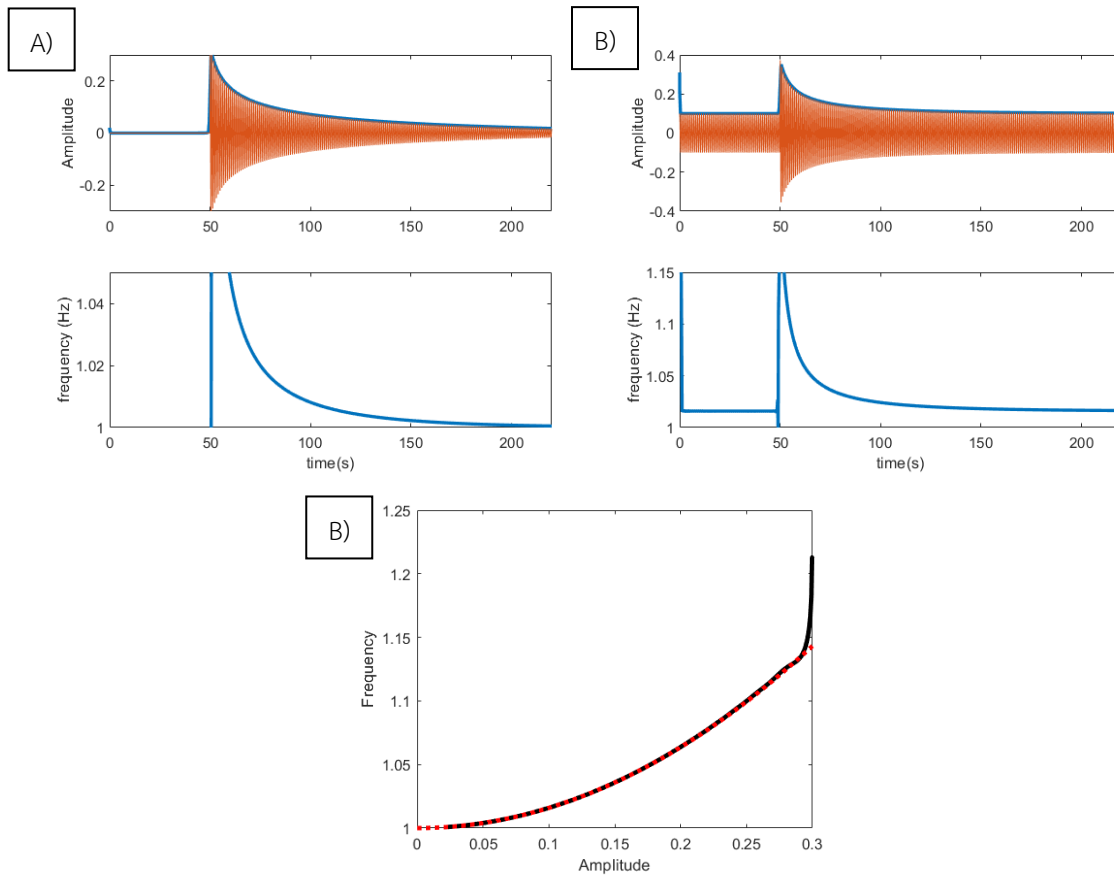
Figure 4.9 (A) (top panel) The displacement of an oscillator perturbed by a transient force of XX seconds (orange line) and the instantaneous amplitude (blue line). (Bottom panel) The instantaneous frequency decayed with the amplitude. The oscillator was poised in the stable regime ($\mu < 0$). (B), same as (A), with the oscillator poised in the limit-cycle regime ($\mu > 0$). (C) The instantaneous frequency and amplitude from (A). Red dotted line describes $\omega = \omega_0 - \beta R^2$.

After that, we replace the transient force with a stationary noise term with $D = 1$. We found that the instantaneous frequency increased with the instantaneous amplitude (**Figure 4.10**). The relationship agreed with the equation (4.1).
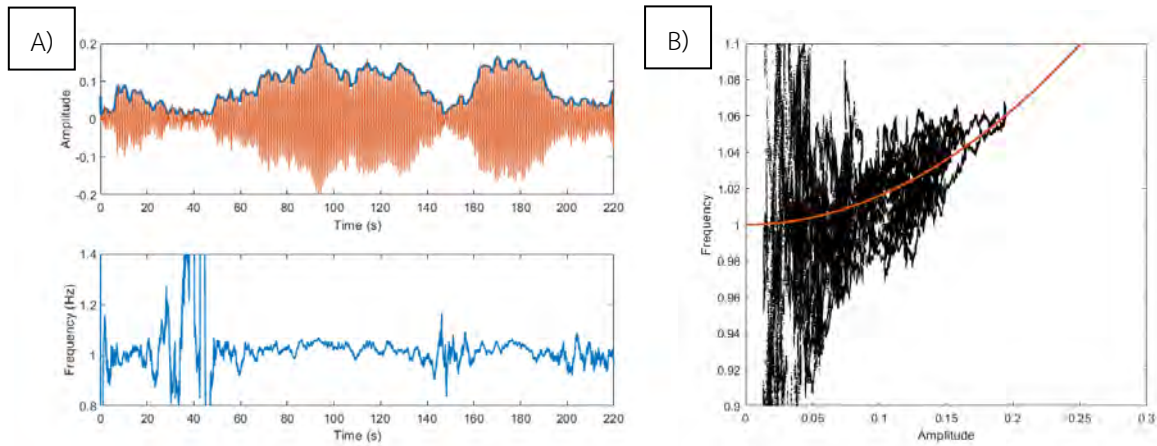
Figure 4.10 A) The instantaneous amplitude (top panel) and instantaneous frequency (bottom panel) when noise term was applied. B) the instantaneous frequency and amplitude from A). The red dot line is $\omega = \omega_0 - \beta R^2$.

4.5 Noise-induced oscillation near a supercritical Hopf bifurcation

We included a noise term to the normal form equation of the supercritical Hopf bifurcation. The control parameter (μ) was fixed at -0.1, thus poising the system in the stable regime near the bifurcation. The characteristic frequency (ω_0) was 10π, and the parameter that governed the degree of nonisochronicity (β) was -10. In the absence of noise, the system remained stationary. When the noise amplitude (D) was increased, the system displayed an oscillation with a distinct peak emerged in the amplitude spectrum. **Figure 4.11** shows that the center frequency increased with the noise intensity.
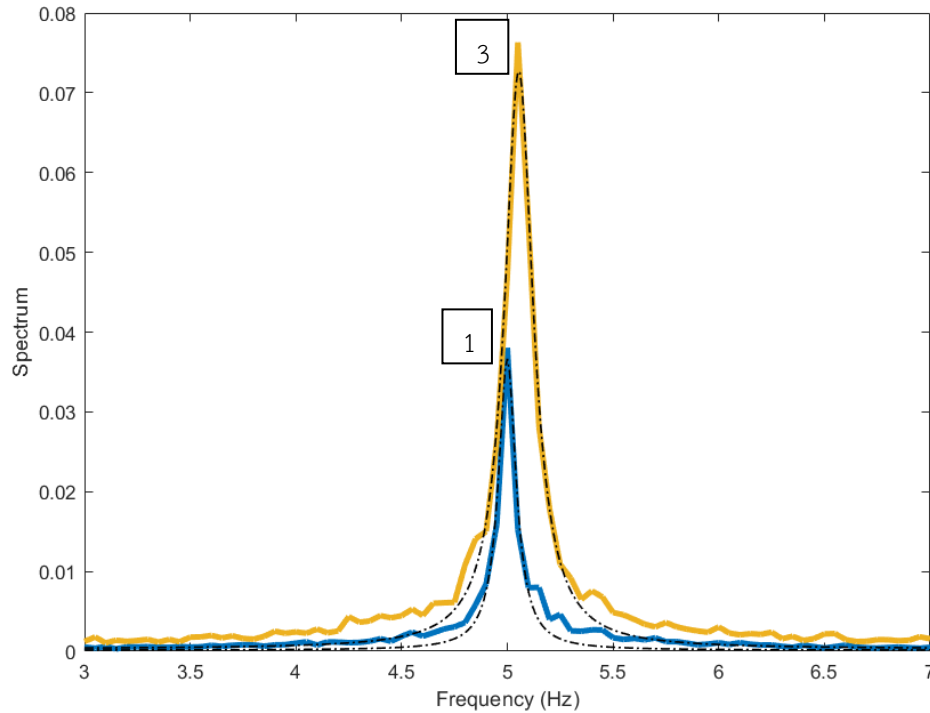
Figure 4.11 The spectrum of $x(t)$ at 2 values of noise amplitude D = 1 (blue line), and D=3, (yellow line). The dashed lines show the Lorentzian equation fitted to the peak.

4.6 The effects of noise intensity

To capture the frequency shift from the experimental results, we varied the noise intensity and extracted the center frequencies of the peaks. As the noise intensity varies with a square root of temperature, we plotted the center frequency against the squared noise intensity, defined as the effective temperature. The relationship between the center frequency and the effective temperature was nonlinear with the shift magnitude declined when the noise intensity increased. To extract the temperature sensitivity, we fitted the frequency over the range of effective temperature between 4 to 64 and defined the slope as a temperature sensitivity. The characteristic frequency ω_0 only minimally influenced the temperature sensitivity (**Figure 4.12**).

As the effective temperature level increased, the amplitude of the noise-induced motion became greater, and the oscillation became more irregular. **Figure 4.13** shows that the peak width increased with the peak height.
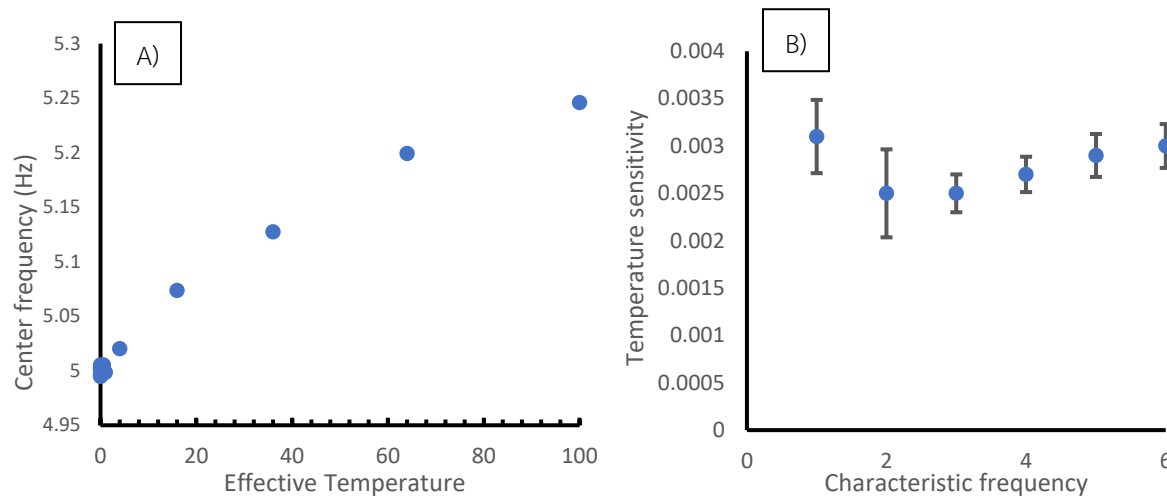

Figure 4.12 A) The center frequency increased with the effective temperature. The frequency shift was lower at a higher effective temperature. B) The relationship between the temperature sensitivity and the characteristic frequency was relatively flat.

4.7 The effects of real noise and complex noise terms

We investigated the differences between real noise and complex noise. We compared their effects on the center frequency, peak height, and width. **Figure 4.14** shows that, within the range of parameters investigated in our work, both types of noise had qualitatively similar effects on the peak characteristics. The complex noise seemed to have stronger effect than real noise.

4.8 the preliminary results of the system in oscillation regime

In this final section we present preliminary results of the effects of noise on the oscillatory system. The noise term was added to the system which had $\mu = 0.1$. Similar results were observed: the center frequency and width increased with noise intensity within the range of noise intensity explored. However, there existed a broad tuning in the peak height as a function of noise intensity.

Although this roughly coincided with the experimental results, the width of the spectral peaks remained relatively constant within the same range of noise intensity.

Figure 4.13 A) The relationship between the peak width and B) the peak height and effective temperature. C) The width and the peak height displayed a positive correlation.
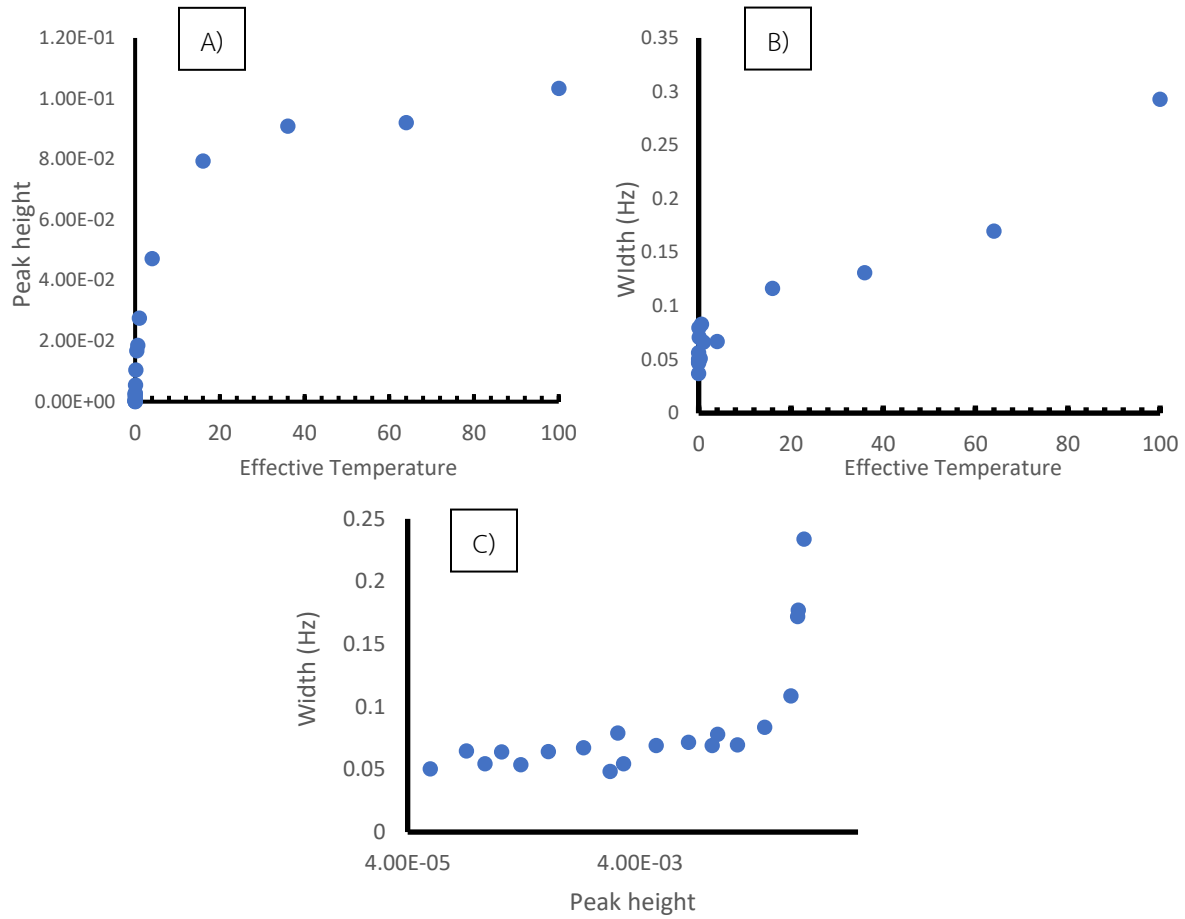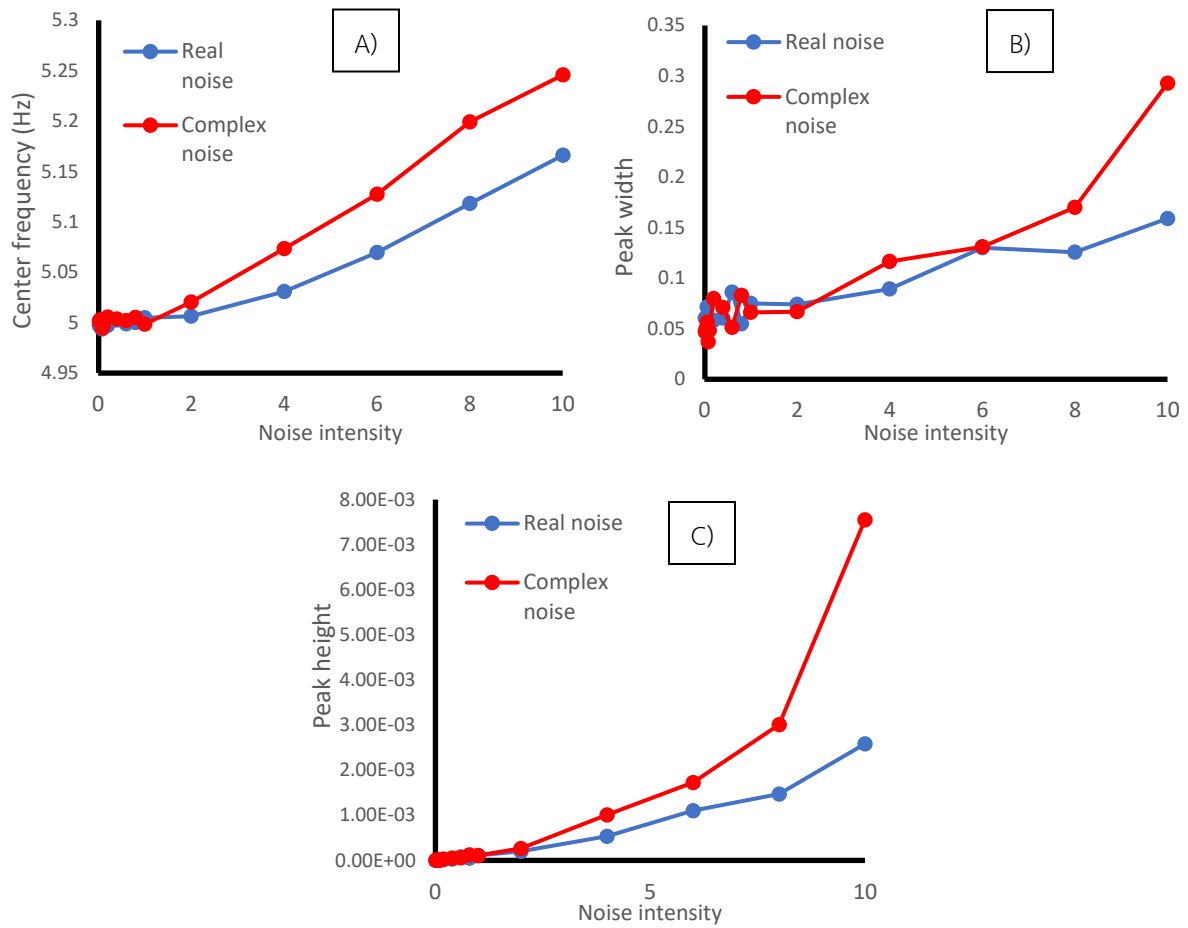
Figure 4.14 The effects of real and complex noise on A) the center frequency, B) the peak width, and C) the peak height.
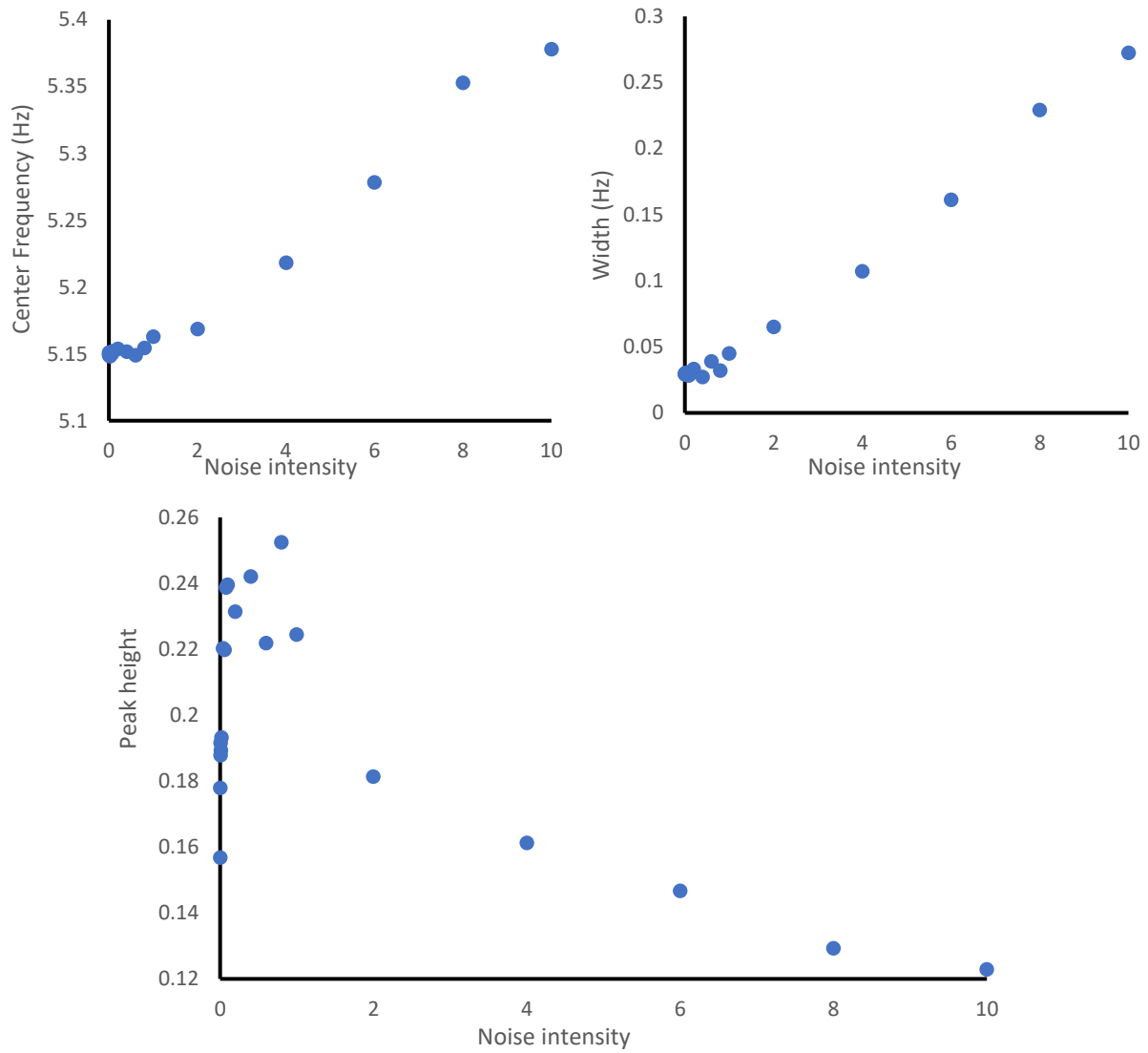
Figure 4.14 the results in oscillation regime show the similarity to quiescent regime except for the peak height that present a broad peak relationship.

Chapter 5

Discussion and Conclusion

5.1 Discussion

From a perspective of a nonlinear dynamical system near a bifurcation, the motion of hair-cell bundles which underlies the generation of SOAEs is strongly influenced by random fluctuations. In this work, we manipulate the noise level by changing the body temperature and investigate its effects on SOAE peaks in the amplitude spectrum. An SOAE peak is characterized with its center frequency, the 0.5-dB peak width, and its peak height relative to the noise floor.

In agreement with previous works in frogs [12,13] and lizards [6,14,22], our experimental observations reveal that the center frequency increases with body temperature. The sensitivity shows an exponential growth with the peak frequency. This frequency shift behavior is consistent with a non-isochronous nonlinear oscillator near a supercritical Hopf bifurcation. Results from numerical simulations show that the peak frequency increases with the effective temperature. Analysis of equation (3.3) suggests that the change in the peak frequency is dictated by the amplitude of the oscillation. As the effective temperature increases, the average amplitude of oscillation becomes larger resulting in an increase in the average frequency. In contrast to the experiment, however, the frequency sensitivity is minimally dependent on the characteristic frequency of the oscillator.

We find that the thermal effects on the width and the height of SOAE peaks are inconclusive. An increase in the temperature may enhance or reduce the sharpness and amplitude of the peaks. However, as some peaks display a tuning behavior with a minimal width and a highest amplitude observed over a certain range of temperature, we speculate that an individual SOAE peak possesses a characteristic optimal temperature at which the signal becomes most coherent. This optimal temperature could be out of the range achieved in our experiments. This implies that SOAEs may be produced via a coherence resonance: a noise-induced oscillation

of a system near a bifurcation displays highest degree of coherence over a range of noise intensity. Within the range of parameters investigated in our model, however, the peak width and height increase with the effective temperature. We have not observed a coherence resonance behavior.

The width and height of SOAE peaks displayed a negative correlation, similar to results from human and some lizard species [23,24]. Our model, in contrast, shows that the peak width increases with the peak amplitude.

In summary, our experimental findings confirm that SOAE frequency is dependent on the body temperature and further suggest that SOAEs could be consistent with a coherence resonance. A non-isochronous nonlinear oscillator near a supercritical Hopf bifurcation can describe the shift of SOAE frequencies. This suggests the nonisochronicity of hair-cell bundles which underlies the production of SOAEs. However, our numerical results cannot reproduce the dependence of the temperature sensitivity on the characteristic frequency. In addition, the model cannot predict the effects of changes in the body temperature on width and peak height.

5.2 Suggestions and future work

Experiment: We controlled the temperature using a heating lamp with no temperature setting. Therefore, the temperature level cannot be maintained at a certain level. The limited range of temperature is due to the power of the heating lamp, and the size of the acrylic box. To increase the range of temperature and have more stable temperature, we suggest using a smaller box and a controllable heat source.

Model: The proposed model cannot describe the effects of body temperature on the characteristics of SOAEs. Alternative models include a system of coupled oscillators, and a model of a single hair bundle based on the physiological processes of the bundle.

Bibliography

1. C. Abdala, P. Luo, C. A. Shera. 2017. Characterizing spontaneous otoacoustic emissions across the human life span. J. Acoust. Soc. Am. 141 (3), 1874-1886.

2. Zurek, P. M. 1985. Acoustic emissions from the ear: a summary of results from humans and animals. J. Acoust. Soc. Am. 78, 340–344.

3. Taschenberger, G., and G. A. Manley. 1997. Spontaneous otoacoustic emissions in the barn owl. Hear. Res. 110, 61–76.

4. G. A. Manley, A. Wartini, G. Schwabedissen and E Siegl. 2018 Spontaneous otoacoustic emissions in teiid lizards. Hear. Res. 363, 98-108.

5. P. van Dijk, P. M. Narins, and J. Wang. 1996. Spontaneous otoacoustic emissions in seven frog species. Hear. Res. 101, 102–112.

6. C. Köppl, and G. A. Manley. 1993. Spontaneous otoacoustic emissions in the bobtail lizard. I: General characteristics. Hear. Res. 71, 157–169.

7. Zurek, P. M. 1981. Spontaneous narrowband acoustic signals emitted by human ears. J. Acoust. Soc. Am. 69, 514–523.

8. F. Fruth, F. Jülicher, B. Lindner. 2014. An Active Oscillator Model Describes the Statistics of Spontaneous Otoacoustic Emissions. Biophysical Journal 107, 815-824.

9. J. Tinevez, F. Jülicher, P. Martin. 2007. Unifying the Various Incarnations of Active Hair-Bundle Motility by the Vertebrate Hair Cell. Biophysical Journal 93, 4053-4067.

10. C A Shera. 2003. Mammalian spontaneous otoacoustic emissions are amplitude-stabilized cochlear standing waves. J. Acoust. Soc. Am. 114 (1), 244-262.

11. O.V Ushakov, H.-J. Wünsche, F. Henneberger, I.A. Khovanov, L. Schimansky-Geier, M.A. Zaks. 2005. Coherence Resonance Near a Hopf Bifurcation. PRL 95, 123903.

12. P. van Dijk, H. P. Wit. 1987. Temperature dependence of frog spontaneous otoacoustic emissions. Acoust. Soc. Am. 82 (6), 2147-2150.

13. G. R. Long, P. van Dijk, H. P. Wit. 1996. Temperature dependence of spontaneous otoacoustic emissions in the edible frog (Rana esculenta). Hear. Res. 98, 22-28.

14. G. A. Manley, L. Gallo, C. Köppl. 1996. Spontaneous otoacoustic emissions in two gecko species Gekko gecko and Eublepharis macularius. Acoust. Soc. Am. 99 (3), 1588-1603.

15. P. Martin, D. Bozovic, Y.Choe, A, J, Hudspeth. 2003. Spontaneous Oscillation by Hair Bundles of the Bullfrog's Sacculus. J. Neurosci 23 (11), 4533-4548.

16. A. Vilfan, T. Duke. 2008. Frequency Clustering in Spontaneous Otoacoustic Emissions from a Lizard's Ear. Biophysical Journal 95 (10), 4622-4630.

17. A. J. McKane, T. J. Newman. 2005. Predator-Prey Cycles from Resonant Amplification of Demographic Stochasticity. PRL 94, 218102.

18. G. A. Manley, D.L. Kirk. 2005. BAPTA induces frequency shifts in vivo of spontaneous otoacoustic emissions of bobtail lizard. Audiol Neurootol 10 (5), 248-257.

19 B. Nadrowski, P. Martin, F. Jülicher, A. J. Hudspeth. 2004. Active Hair-Bundle Motility Harness Noise to Operate near Optimum of Mechanosensitivity. PNAS 101, 12195-12200.

20. A. J. Hudspeth. 2014. Integrating the active process of hair cells with cochlear function. Nature 15, 600-614.

21. M. Gelfrand, O. Piro, M. O. Magnasco, A. J. Hudspeth. 2010. Interactions between Hair Cells Shape Spontaneous Otoacoustic Emissions in a Model of the Tokay Gecko's Cochlea. PLoS ONE 5, 1-12.

22. Y. Roongthumskul, D.O. Maoiléidigh, A. J. Hudspeth. 2019. Bilateral Spontaneous Otoaciustic Emissions Show Coupling between Active Oscillators in the Two Ears. Biophysics Journal 116,1-12.

23. P. van Dijk, B. Maat, E de Kleine. 2011. The Effect of Static Ear Canal Pressure on Human Spontaneous Otoacoustic Emissions: Spectral Width as a Measure of the Intra-cochlear Oscillation Amplitude. JARO 12,13-28.

24. P. van Dijk, G. A. Manley. 2015. The Effects of Air Pressure on Spontaneous Otoacoustic Emissions of Lizards. JARO 14, 309-319.

25. V.M. Eguíluz, M. Ospeck, Y. Choe, A.J. Hudspeth, M.O. Magnasco. 2000. Essential Nonlinearities in Hearing. PRL 84 (22), 5232-5235.

26. P. Martin, A.J. Hudspeth. 2001. Active hair-bundle movements can amplify a hair cell's response to oscillatory mechanical stimuli. PNAS 96 (25), 14306-14311.

27. D. Ó Maoiléidigh, E.M. Nicola, A. J. Audspeth. 2012. The diverse effects of mechanical loading on active hair bundles. PNAS 109 (6), 1943-1948.

28. J. D. Salvi, D. Ó Maoiléidigh, B. A. Fabella, M. Tobin, A. J. Hudspeth. Control of a hair bundle's mechanosensory function by its mechanical load. PNAS 112 (9), E1000-E1009.

29. J. D. Salvi, D. Ó Maoiléidigh, A. J. Hudspeth. 2016. Identification of Bifurcations from Observations of Noisy Biological Oscillators. Biophysics Journal 111, 798-812.

30. World Heath Organization. 2018. WHO global estimate on prevalence of hearing loss.

Appendix

Table A1 the body weight and dates of recording of geckoes

Date of recording	Body weight (g)
8/26/2019	66
9/3/2019	130
9/9/2019	82
10/23/2019	60
12/18/2019	77
1/16/2019	72